Quantum Physics Letters
An International Journal

http://dx.doi.org/10.18576/qpl/090301

Comparative Study of Asymmetric Nuclear Matter using Extended BHF with Different Types of Three-Nucleon Forces

H. M. Abou-Elsebaa[1,2]

[1]Physics Department, College of Science, Taibah University, Medina 41411, Saudi Arabia
[2]Physics Department, Faculty of Science, Sohag University, Sohag 82524, Egypt

Received: 5 Aug. 2020, Revised: 15 Nov. 2020, Accepted: 23 Nov. 2020
Published online: 1 Dec. 2020

Abstract: The equation of state for asymmetric nuclear matter, the symmetry energy and proton fraction are calculated utilizing the microscopic many-body Brueckner-Hartree-Fock approach using the CD-Bonn and Argonne V_{18} nucleon-nucleon potentials enhanced with various types of three-body forces. These models are constructed to reproduce the experimental value of binding energy of symmetric nuclear matter. In addition, three-body forces are likely crucial in the case of dense nuclear matter to obtain a stiff equation of state to reproduce the maximum mass of the neutron stars compatible with the measured experimental values.

Keywords: Symmetric nuclear matter, Equation of State, Symmetry energy, Proton Fraction, Three-body forces, Neutron stars.

1 Introduction

The equation of state (EOS) of asymmetric nuclear matter (ANM) is a long-standing issue in both nuclear physics and astrophysics. Different methodologies including diverse actual approximations and mathematical methods have been created to manage the many-body issue of isospin-asymmetric nuclear matter. The properties of asymmetric nuclear matter are of major significance in heavy ion collisions, neutron star structure and nuclear astrophysics [1].

The properties of neutron stars rely upon the EOS at densities higher than those observed in ordinary situations. Information on the EOS can be acquired from numerous sources, for example, studies of the monopole resonance in finite nuclei, high-energy nuclear collisions, supernova and neutron stars. Supernova simulations appear to require an EOS which is too soft to support some observed masses of neutron stars, while analysis of high-energy nuclear collisions demonstrate a fairly stiff EOS, predicting neutron star masses which are too large [2].

Study the density reliance of the nuclear symmetry energy has been the primary focal point of the intermediate-energy heavy-ion physics community during the most recent decade, and huge progress has been achieved both experimentally and theoretically. Information on the nuclear symmetry energy is fundamental for understanding not only many problems in nuclear physics, such as the dynamics of heavy-ion collisions induced by radioactive beams and the structure of exotic nuclei, but also a number of important issues in astrophysics, such as the nucleosynthesis during pre-supernova evolution of massive stars and the cooling of protoneutron stars. Albeit the nuclear symmetry energy at normal nuclear matter density is known to be around 30 MeV from the empirical liquid-drop mass formula [3], its values at other densities, especially at supra-normal densities, are poorly known [4].

A better understanding of the composition of nuclear matter at the highest densities has important implications not only in nuclear physics, but also in relativistic astrophysics, the composition of dense nuclear matter in the high density (deep interior) of neutron stars is still largely unknown. Several EOSs for neutron star matter have been proposed theoretically, However, the discoveries of $2M_{\odot}$ neutron stars ruled out most of the soft EOSs, for which the maximum mass can not reach the observed $2M_{\odot}$ [5]. The maximum mass of neutron stars depends strongly on the stiffness of the EOS [6].

* Corresponding author e-mail: h.abualsba@science.sohag.edu.eg

This paper is organized as follows. In section II, we will describe the formalisms within the non-relativistic approaches we have employed. Results for the EOS, symmetry energy and proton fraction for asymmetric nuclear matter using the suggested models, together with neutron star matter observables will be presented in sect. III. A short summary and some conclusions will be given in sect. IV.

2 Theoretical Model

For asymmetric nuclear matter with neutron density ρ_n, proton density ρ_p, total density $\rho = \rho_n + \rho_p$ and isospin asymmetry $\beta = \frac{\rho_n - \rho_p}{\rho}$, one has different G-matrices describing the nn, pp and np in medium effective interactions, they are obtained by solving the well-known Bethe-Goldstone equation [7,8].

$$G_{\tau_1\tau_2;\tau_3\tau_4}(\omega) = V_{\tau_1\tau_2;\tau_3\tau_4} + \sum_{ij} V_{\tau_1\tau_2;\tau_i\tau_j} \frac{Q_{\tau_i\tau_j}}{\omega - \varepsilon_{\tau_i} - \varepsilon_{\tau_j} + i\varepsilon} \times G_{\tau_i\tau_j;\tau_3\tau_4}(\omega) \quad (1)$$

where τ_q (q = 1, 2, i, j, 3, 4) indicates the isospin projection of the two nucleons in the initial, intermediate and final states, V is the bare NN interaction, $Q_{\tau_i\tau_j}$ is the Pauli operator and ω is the starting energy corresponds to the sum of non-relativistic energies of the interacting nucleons.

The single-particle energy $\varepsilon_\tau(k)$ of a nucleon with momentum k and mass m_τ is given by:

$$\varepsilon_\tau(k) = \frac{\hbar^2 k^2}{2m_\tau} + Re[U_\tau(k)] \quad (2)$$

where $U_\tau(k)$ is the single-particle potential. In the BHF approximation, $U_\tau(k)$ is calculated from the equation:

$$U_\tau(k) = \sum_{\tau'} \sum_{k' < k_{F_{\tau'}}} < kk' \mid G_{\tau\tau';\tau\tau'}(\omega = \varepsilon_\tau(k) + \varepsilon_{\tau'}(k')) \mid kk' >_A \quad (3)$$

the sum runs over all n and p occupied states and the matrix elements are properly anti-symmetrized, a self-consistent solution of Eqs. (1) - (3) is achieved, E/A can be calculated as

$$\frac{E}{A}(\rho,\beta) = \frac{1}{A}\sum_{\tau}\sum_{k<k_{F_\tau}} \left(\frac{\hbar^2 k^2}{2m_\tau} + \frac{1}{2}Re[U_\tau(k)]\right) \quad (4)$$

The phenomenological Urbana interaction has been used to study the effect of 3BFs on the EOS. It consists of two terms one is an attractive term due to two-pion exchange with excitation of an intermediate Δ resonance, the other is a repulsive phenomenological central term, the 3BF is written as [9].

$$V_{ijk} = V_{ijk}^{2\pi} + V_{ijk}^{R} \quad (5)$$

Another way is by adding the effective interaction or the self-energy of BHF calculations by a simple contact interaction, which we have chosen following the notation of the Skyrme interaction to be in the form [10],

$$\Delta(\frac{E}{A}) = CT = \frac{3}{8}t_0\rho + \frac{3}{48}t_3\rho^{\sigma+1} \quad (6)$$

The parameters t_0 and t_3 represent the zero range and 3 -body strength while the exponent σ determines the high density behavior. We take σ = 0.33, 0.5, 0.67, we have fitted t_0 and t_3 in such a way that BHF calculations plus the contact term (CT) yield the empirical saturation point for SNM.

The asymmetric nuclear matter properties can be extracted by interpolating the two extreme situations of SNM and pure neutron matter (PNM) with the empirical parabolic approximation [11]:

$$\frac{E}{A}(\rho,\beta) = (1-\beta^2)\frac{E}{A}(\rho,0) + \beta^2\frac{E}{A}(\rho,1) \quad (7)$$

The EOS of PNM joined with that of SNM gives us information on the isospin impacts specifically on the symmetry energy a_s [12]. The symmetry energy of nuclear matter is defined as the second derivative of energy per nucleon E/A with respect to the asymmetry parameter β as follows

$$a_s(\rho) = \frac{1}{2}\left[\frac{\partial^2 E/A(\rho,\beta)}{\partial\beta^2}\right]_{\beta=0} \quad (8)$$

in good approximation, the symmetry energy can be expressed in terms of the difference of the energy per nucleon between SNM(β = 0) and PNM (β = 1):

$$a_s(\rho) = \frac{E}{A}(\rho,1) - \frac{E}{A}(\rho,0) \quad (9)$$

The β^2– law of the EOS Eq. (7) of ANM at any isospin asymmetry leads to important consequence, it indicates that the EOS of ANM at any isospin asymmetry is given completely by the EOS of SNM and the symmetry energy [13]:

The proton fraction x_p related to the symmetry energy by the equation [14]

$$x_p \simeq \frac{64a_s(\rho)^3}{3\pi^2(c)^3 + 128a_s(\rho)^3} \quad (10)$$

To calculate the properties of neutron stars, one starts from the Tolman-Oppenheimer-Volkov (TOV) equations for the total pressure P and the enclosed mass m [15,16],

$$\frac{dP}{dr} = \frac{-G[m(r) + 4\pi^3 P/c^2][\varepsilon + P/c^2]}{r[r - 2Gm(r)/c^2]}, \quad (11)$$

$$\frac{dm(r)}{dr} = 4\pi\varepsilon r^2 \quad (12)$$

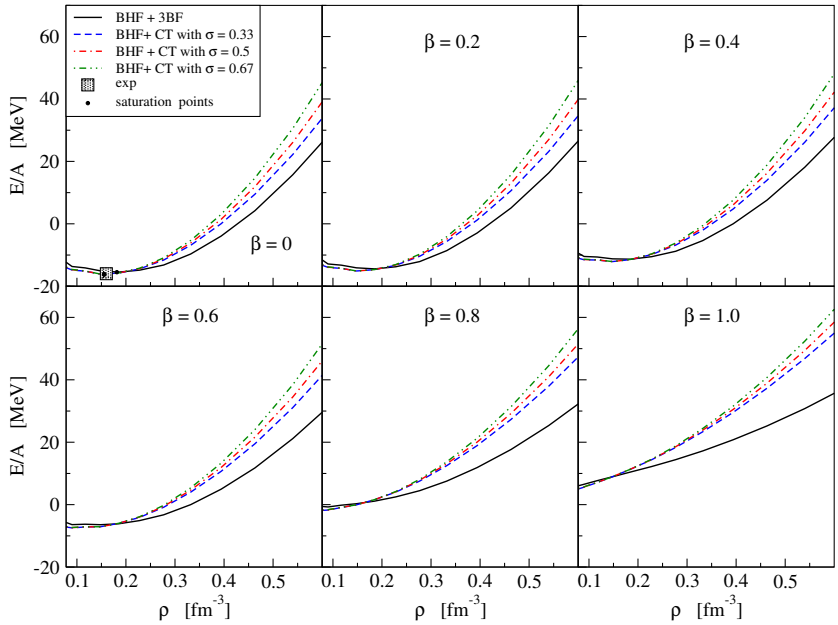

Fig. 1: (color online) E/A in MeV for ANM as a function of ρ in fm^{-3} at different values of asymmetry parameter β using CD-Bonn potential. The black solid lines correspond to BHF + 3BF results while blue dashed lines correspond to BHF+CT with σ = 0.33 results, also red dash-dotted lines correspond to BHF+CT with σ = 0.5 and green dash-double-dotted lines correspond to BHF+CT with σ = 0.67. The empirical saturation point is given by the big black square and the black solid points indicate the saturation points of each interaction.

where $P(r)$ is the pressure at radius r, $m(r)$ is the gravitational mass inside r, and G is the gravitational constant. From the EOS of asymmetric nuclear matter, we can calculate the pressure P of stellar matter and the total mass density ε using the relations,

$$P = \rho^2 \frac{d\mathscr{E}_{tot}}{d\rho}, \tag{13}$$

$$\varepsilon = \rho \cdot \mathscr{E}_{tot}/c^2, \tag{14}$$

where c is the speed of light in vacuum. Starting with a central mass density $\varepsilon(r=0) \equiv \rho_c$, one can integrate out until the pressure on the surface equals the one corresponding to the density of iron. This gives the stellar radius R and the gravitational mass M_G:

$$M_G \equiv m(R) = 4\pi \int_0^R dr\, r^2 \rho(r). \tag{15}$$

To calculate the total mass and radius of neutron star, we employ the EOS defined in Eqs. (13) and (14) with the boundary conditions

$$P_c = P(\rho_c), \qquad M(0) = 0,$$

where the subscript c refers to the center of the star, and ρ_c is the central density which is our input parameter in the calculations of neutron star properties.

3 Results and Discussion

3.1 The EOS for ANM

We start the discussion with the EOS for ANM results, it is considered as an important ingredient in studying the properties of nuclei far from stability, also is crucial for determining the properties of one of the most exotic objects in the universe neutron stars and studying the structures of compact astrophysical objects, such as the core-collapse supernova. In Fig. 1, the binding energy per nucleon (E/A) as a function of density at several values of asymmetry parameter β predicted using the CD-Bonn potential for different approaches, we calculate the results at β = 0 (SNM), 0.2, 0.4, 0.6 (ANM), 1.0 (PNM). The black solid lines correspond to BHF + 3BF results while blue dashed lines correspond to BHF+CT with σ = 0.33 results, also red dash-dotted lines correspond to BHF+CT with σ = 0.5 and green dash-double-dotted lines correspond to BHF+CT with σ = 0.67. The empirical saturation point is given by the big black square and the black solid points indicate the saturation points of each interaction.

The results for E/A first decreases with increasing density until it reach a minimum called the saturation point, then it increase with increasing density. The left upper panel correspond to SNM (β = 0), the inclusion of the 3BF contribution improves the saturation properties to

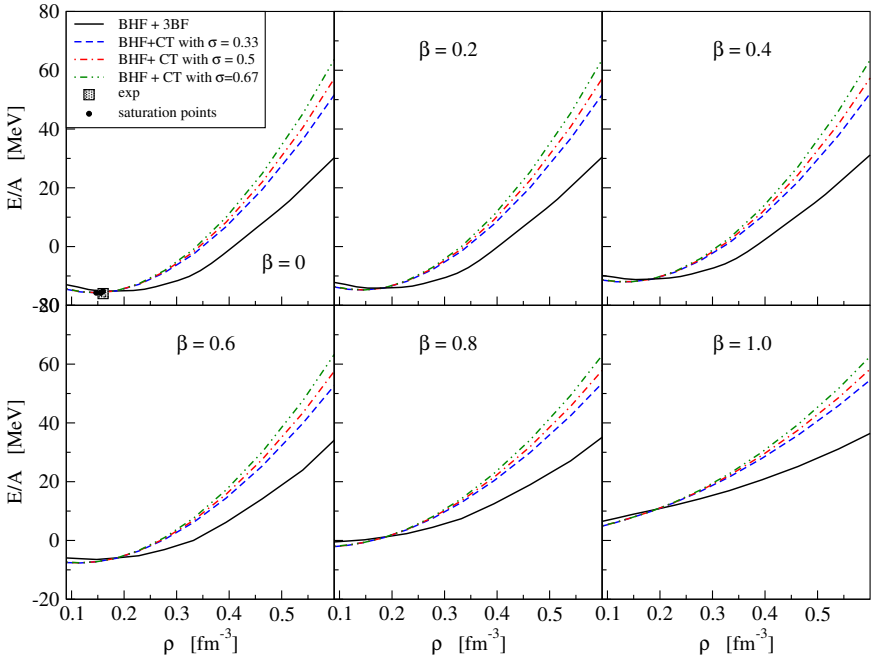

Fig. 2: (Color online) The same as Fig.1 but using Argonne V_{18} potential.

be close to the empirical one. When we add the contact term to the BHF approximation our EOS models are able to reproduce the empirical saturation point of SNM. The empirical saturation point for SNM given by (ρ_0=0.17±0.01 fm^{-3}, E_0/A = -16 ±1 MeV). As the value of the asymmetry parameter increases, we find that the values of the E/A become more repulsion until we reach the state of the pure neutron matter, at which the values of E/A take only positive values.

Comparing the results, the inclusion of the CT to BHF approach increases the repulsion of EOS. At low density the results are close to each other, at high density some differences occur between the three curves, this means that the BHF + CT effect is found to become sizable at high densities above the saturation density. When we use BHF+CT with σ = 0.67 the results are more repulsion than the other cases. It is clear that the EOSs using BHF+CT with σ = 0.67 are stiffer than the EOSs results by using BHF+CT with σ = 0.33. The results for the EOS of ANM is strongly increased when CT term is introduced, this is true not only around saturation but also throughout a wide range of density.

In Fig. 2 the same as Fig. 1 but using Argonne V_{18} potential, the results for Argonne V_{18} potential are more repulsion than these for CD-Bonn potential. The reason for the difference in results between the two potentials used lies in that the Argonne V_{18} potential is a local potential, while CD-Bonn potential is nonlocal potential.

The values of the saturation points have been evaluated for all the present approaches of SNM for the two interaction models and are listed in Table 1. One may notice that the calculations are in reasonable agreement with the experimental data.

3.2 Symmetry energy and proton fraction

The nuclear symmetry energy is the energy difference between removing a proton or a neutron from nuclear matter [17], it is calculated using equation (9), it is equal to the difference in E/A for pure neutron matter and symmetric nuclear matter. In Fig. 3, the results for the symmetry energy a_s as a function of ρ are showed, left panel using CD-Bonn potential, right panel using Argonne V_{18} potential at three values of the CT=0.33, 0.5 and 0.67. The results first increase with increasing density until it reach a maximum value then it begins to decrease with increasing density. The values of a_s are similar to each other at low ρ, with significant difference occurred at higher ρ. This means that at low density a_s is largely independent of the interaction used, V_{18} potential leads to a symmetry energy which, at high densities is even lower than the CD-Bonn results. The CD-Bonn potential reaches to a maximum value of the symmetry energy at higher density comparing with the Argonne V_{18} potential because it is a nonlocal potential. The Argonne V_{18} potential is a stiffer interaction and predicts less symmetry energy than the softer CD-Bonn potential.

The proton fraction X_p is calculated using equation (10), in Fig. 4, the results for the proton fraction X_p as a function of ρ in fm^{-3} are discussed, left panel using CD-Bonn potential right panel using Argonne V_{18}

Table 1: The saturation densities ρ_0 and the saturation energies (E/A).

	CD-Bonn		Argonne V_{18}	
Model	ρ_0 $[fm^{-3}]$	E/A [MeV]	ρ_0 $[fm^{-3}]$	E/A [MeV]
BHF+3BF	0.1815	-15.496	0.15	-15.227
BHF+CT with σ=0.33	0.17	-16	0.17	-16
BHF+CT with σ=0.5	0.17	-16	0.17	-16
BHF+CT with σ=0.67	0.17	-16	0.17	-16
Empirical sat. point	0.17±0.01	-16±1	—	—

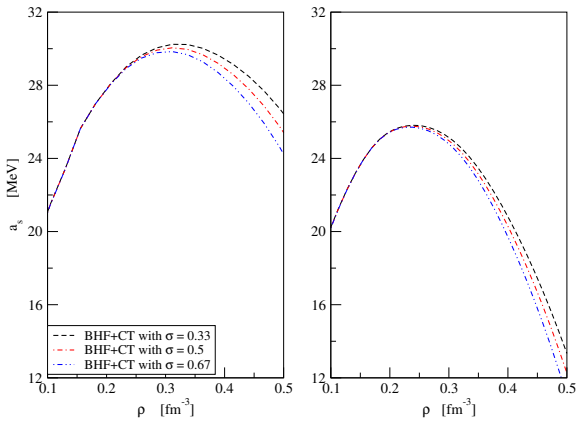

Fig. 3: (Color online) The density dependence of symmetry energy a_s, left panel using CD-Bonn potential right panel using Argonne V_{18} potential.

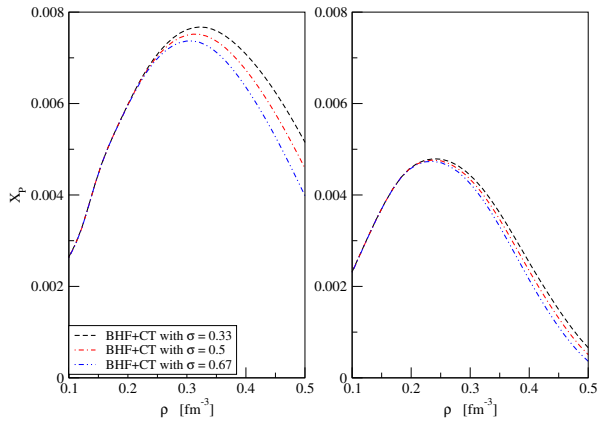

Fig. 4: The proton fraction X_p as a function of ρ in fm^{-3}, left panel using CD-Bonn potential right panel using Argonne V_{18} potential.

potential. From the figure we note that X_p take small values between 0.002 and 0.008, the results increase with increasing density until it reach a maximum value, then it decrease with increasing density. the results for the Argonne V_{18} potential are less than that for CD-Bonn potential at the same ρ.

3.3 Neutron Stars Properties

It is believed that macroscopic portions of asymmetric nuclear matter form the interior bulk part of neutron stars, commonly associated with pulsars. Despite the fact that infinite nuclear matter is obviously an idealized physical system, the theoretical determination of the corresponding EOS is an essential step towards the understanding of the physical properties of neutron stars. In this section, We analyze how the EOS affects several neutron star properties and how it impacts on possible constraints inferred from astrophysical observations and we examine the maximum mass limit of neutron stars using ANM at $\beta = 0.6$. In Fig. 5, the results for neutron star gravitational mass M_G (in units of $M_\odot = M_{sun}$) plotted as a function of the central density ρ_c in units of gm/cm^3, left panel using CD-Bonn potential right panel using Argonne V_{18} potential.

In Fig. 6, the results for neutron star gravitational mass M_G (in units of $M_\odot = M_{sun}$) plotted as a function of the stellar radius in units of km, left panel using CD-Bonn potential right panel using Argonne V_{18} potential. At tables 2 and 3 the values of the maximum gravitational mass M_{max}, radius R and central density ρ_c of the neutron star are listed using CD-Bonn potential and Argonne V_{18} potential, respectively by ANM at $\beta = 0.6$.

The EOS of dense matter must be stiffness enough in order to support such large masses. In the right panel we observe that the maximum mass limit of the neutron stars is larger than the corresponding limit in the left panel. As the value of the CT increases the maximum mass limit increases also. By CD-Bonn potential, the calculated values for the maximum mass using BHF+CT with σ=0.5 are slightly smaller than the experimental data, also, the calculated values for the maximum mass using BHF+CT with σ=0.67 is consistent with the masses calculated by PSRs J1614-2230=1.97 $\pm$ 0.04 [18] and J0348+0432=2.01 $\pm$ 0.04 [19].

Our results using Argonne V_{18} potential, at BHF+CT with σ=0.5 and BHF+CT with σ=0.67 are consistent with the masses calculated by PSRs J1614-2230=1.97 $\pm$ 0.04 [18] and J0348+0432=2.01 $\pm$ 0.04 [19].

Table 2: The maximum gravitational mass M_{max}, radius R and central density ρ_c of the neutron star are calculated using CD-Bonn potential for ANM at $\beta = 0.6$.

Model	M_{max} $(M_\odot)$	$\rho_c \times 10^{15}(gm/cm^3)$	R (km)
BHF+CT with σ=0.33	1.7345	4.46	8.1509
BHF+CT with σ=0.5	1.871	4.46	8.2681
BHF+CT with σ=0.67	2.0225	3.98	8.5769
PSR J1614-2230[18]	1.97 ± 0.04		
PSR J0348+0432[19]	2.01 ± 0.04		

Table 3: Same as Table 2 but using Argonne V18 potential.

Model	M_{max} $(M_\odot)$	$\rho_c \times 10^{15}(gm/cm^3)$	R (km)
BHF+CT with σ=0.33	1.8989	4.47	8.1862
BHF+CT with σ=0.5	2.0123	3.98	8.2991
BHF+CT with σ=0.67	2.1379	3.98	8.3984
PSR J1614-2230[18]	1.97 ± 0.04		
PSR J0348+0432[19]	2.01 ± 0.04		

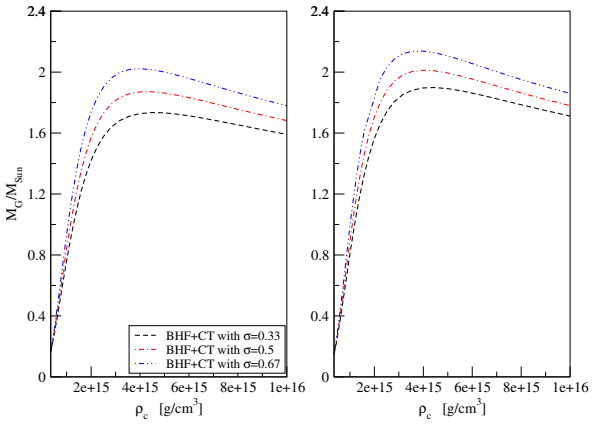

Fig. 5: Neutron star gravitational mass M_G (in units of $M_\odot = M_{sun}$) plotted as a function of the central density ρ_c in units of gm/cm^3 using ANM at $\beta = 0.6$, left panel using CD-Bonn potential right panel using Argonne V_{18} potential.

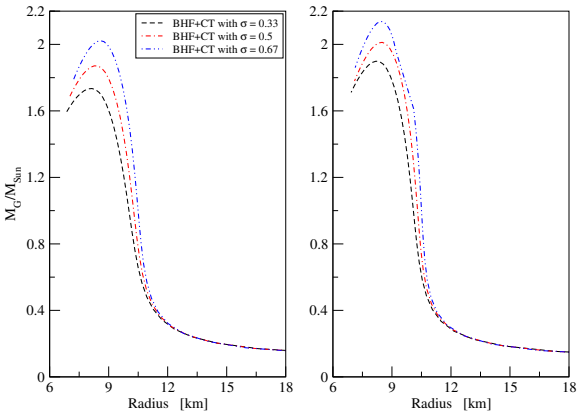

Fig. 6: Predicted neutron star gravitational mass M_G (in units of $M_\odot = M_{sun}$) as a function of the stellar radius in km using ANM at $\beta = 0.6$, left panel using CD-Bonn potential right panel using Argonne V_{18} potential.

4 Conclusion

The EOSs of symmetric, asymmetric, and pure neutron matter have been computed using BHF approximation, BHF + 3BF and BHF +CT at three different values of CT (at σ = 0.33, 0.5, and 0.67). The calculated values of the saturation points are found to be in an excellent agreement with empirical data (ρ_0 = 0.17 fm^{-3}; E_0 = -16 MeV). Also, it is observed that with the increase in the asymmetry parameter β, the EOS becomes stiff and the trend continues until it becomes pure neutron matter.

Also, the neutron stars properties such as their masses and radii are calculated. Our results using the CD-Bonn potential with BHF+CT and σ=0.67 as well as with the Argonne V_{18} potential with BHF+CT and σ=0.5 and BHF+CT with σ=0.67 are consistent with the masses calculated by PSRs J1614-2230=1.97 $\pm$ 0.04 [18] and J0348+0432=2.01 $\pm$ 0.04 [19].

Acknowledgements

I am gratefully acknowledge useful discussions with Prof. Kh. S. A. Hassaneen and Prof. E. M. Darwish. I am deeply indebted to Prof. M. Baldo for providing us with the Computer code for three-body force.

Conflict of Interest

The author declare that there is no conflict of interest regarding the publication of this article.

References

[1] B. A. Li, L. W. Chen and C. M. Ko 2008 Phys. Rep. 464 113
[2] L. Engvik, M. Hjorth-Jensen, E. Osnes, G. Bao and E. Østgaard, Phys. Rev. Lett. **73**, 2650, (1994).
[3] K. Pomorski, J. Dudek, Phys. Rev. C 67 (2003) 044316.
[4] B.A. Li, C.M. Ko, W. Bauer, topical review, Int. Jour. Mod. Phys. E 7 (1998) 147.
[5] P. B. Demorest, T. Pennucci, S. M. Ransom, M. S. E. Roberts, and J.W. T. Hessels, Nature 467, 1081 (2010).
[6] H. Sotani, Phys. Rev. C 95, 025802 (2017).
[7] I. Vidaña and I. Bombaci, Phys. Rev. C **66**, 045801 (2002).
[8] Kh.S.A. Hassaneen and H. Müther, Phys. Rev. C **70**, 054308 (2004).
[9] Baldo and Alaa Eldeen Shaban, Physics Letter B 661, 373 (2008).
[10] P. Gögelein,E. N. E. van Dalen, Kh. Gad, Kh. S. A. Hassaneen,and H. Müther, Phys. Rev. C **79**, 024308 (2009).
[11] Kh. Gad and Kh.S.A. Hassaneen, Nucl. Phys. A **793**, 67-78 (2007).
[12] I. Bombaci and U. Lombardo, Phys. Rev. C **44**, 1892 (1991).
[13] Kh.S.A. Hassaneen and Kh. Gad, J. Phys. Soc. Jpn **77**, 084201 (2008).
[14] A.W. Steiner, J.M. Lattimer, and E.F. Brown, Eur. Phys. J. A **52**: 18 (2016).
[15] J. Oppenheimer and G. Volkoff, Phys. Rev. **55**, 374 (1939).
[16] R.C. Tolman, Proc. Nat. Acad. Sci. USA **20**, 3 (1934).
[17] M. Baldo and G. F. Burgio, Progress in Particle and Nuclear Physics 91, 203 (2016), arXiv:1606.08838 [nucl-th]
[18] P.B. Demorest, T. Pennucci, S.M. Ransom, M.S.E. Roberts, and J.W.T. Hessels, Nature **467**, 1081 (2010).
[19] J. Antoniadis *et al.*, Science **340**, 6131 (2013).